Localized trimers inducing metallic states in sub-monolayer thin Bi films on InSb(111)A

Rohit Yadav [1,2,*] Sandra Benter [1,2,3] and Rainer Timm [1,2,†]

[1]*Division of Synchrotron Radiation Research, Department of Physics, Lund University, 221 00 Lund, Sweden*

[2]*NanoLund, Lund University, 221 00 Lund, Sweden*

[3]*ESRF - European Synchrotron Radiation Facility, 38000 Grenoble, France*

(Received 19 February 2025; revised 12 May 2025; accepted 20 May 2025; published 24 June 2025)

Low-dimensional topological states have transformed our understanding of charge transportation through quantum materials. Many relevant observations have been connected to bismuth (Bi) containing materials or ultrathin Bi films. Here, we studied sub-monolayer amounts of Bi deposition on the In-terminated InSb(111)A surface using various complementary surface science techniques. Bi deposition at elevated sample temperature results in well-ordered (2×2) and $(2\sqrt{3} \times 2\sqrt{3})$-R30° surface reconstructions. Scanning tunneling microscopy/spectroscopy (STM/S) data show an enhanced density of states at the interface of the two reconstructions and local Bi trimers over the (2×2) reconstructed surface. Bi-induced metallic surface states crossing the Fermi level are observed and attributed exclusively to the localized trimer states through STS and angle-resolved photoemission spectroscopy (ARPES) results. Furthermore, the ARPES spectra show band splitting at the Γ point and degenerate surface states at the M point, which is associated with Rashba splitting due to strong Bi-substrate interaction. Thus we interpret the Bi/InSb(111)A, exhibiting spin-split metallic surface states induced by localized Bi structures, as a promising candidate for exploring low-dimensional states and spin dynamics in future quantum materials.

DOI: 10.1103/mp9b-hgz1

I. INTRODUCTION

Bismuth (Bi) and Bi-based alloys have been under investigation due to their extraordinary electronic properties, such as large spin-orbit (SO) coupling, quantum spin Hall effect, and spin splitting [1–3]. Bulk Bi(111) surfaces and free-standing films show nontrivial topological states [4,5], whereas strong Bi film-substrate interaction results in trivial topological states [6,7] and quantum spin Hall systems with a large inverted gap, as observed reported for one-monolayer (ML) thin honeycomb Bi films (also called bismuthene) on SiC [8], Ag(111) [9], Si [10], and GaAs [11]. Strong Bi-substrate intersection and large SO coupling result in broken inversion symmetry, which induces spin-polarized band splitting in nonmagnetic materials, also known as the Rashba-Bychkov effect or simply the Rashba effect [6].

The Rashba effect has been explored for Bi films on substrates with inherent spatial inversion asymmetry, such as those with zinc-blende crystal structures. InSb is such a material with a zinc-blende structure and it provides the largest SO coupling among III-V alloys [12]. Thus recent studies focused on Bi overlayer growth on the InSb(111)B surface (Sb-terminating). For example, Inbar *et al.* investigated the electronic properties of deposited Bi films down to a few BL and observed trivial topological states [13]. Liu *et al.* likewise studied the Bi-induced fractal Sierpiński triangular structure on InSb(111)B [14]. We have also studied the incorporation of Bi on InSb(111)B, observed Bi-induced superstructures containing Bi monomers and trimers, and a self-limiting formation of a Bi-Sb interface layer. [15] However, an investigation of Bi deposition on InSb(111)A and especially of the electronic properties of ultrathin Bi films on InSb(111), with Bi amounts of 1 ML or less, is missing. It is important to associate atomic distribution and structure with electronic properties and band dispersion for advanced low-dimensional properties. This is especially relevant for bismuth, as higher-order topological states and strong electronic correlations on localized edge states have been reported in Bi-induced Sierpiński triangles on InSb(111)B and bismuthene on SiC, respectively [16–18]. Scanning tunneling microscopy and spectroscopy (STM/S) offer atomic-scale insight into these low-dimensional materials. However, complementing it with other techniques, like angle-resolved photoemission spectroscopy (ARPES), is essential to fully understand film-substrate interactions and their impact on the electronic properties of the whole material system.

In this work, we investigate the incorporation of Bi into the InSb(111)A surface using various complementary surface science techniques. STM images show Bi-induced unstrained and well-ordered surfaces, mainly (2×2) and in some places $(2\sqrt{3} \times 2\sqrt{3})$-R30° surface reconstructions. Localized Bi trimer states are observed in the (2×2) reconstructed area

*Contact author: rohit.yadav@sljus.lu.se

†Contact author: rainer.timm@sljus.lu.se

Published by the American Physical Society under the terms of the Creative Commons Attribution 4.0 International license. Further distribution of this work must maintain attribution to the author(s) and the published article's title, journal citation, and DOI. Funded by Bibsam.

and interface states are observed at the border between both reconstructions. These states are only visible in STM images with small sample bias due to an enhanced density of states within the energy region of the bulk band gap, as confirmed by STS. Synchrotron-based x-ray photoemission spectroscopy (XPS) and ARPES measurements show metallic states with a strong indication of Rashba splitting, which can be related to the presence of the Bi trimers, already after the deposition of only 0.3 ML of Bi. Thereby identifying Bi-based localized states that influence the electronic properties of the InSb.

II. METHODS

InSb(111)A wafers from Wafer Technology Ltd., *n*-doped with a Te dopant concentration of 2×10^{14} cm^{-3}, were transferred into the ultrahigh vacuum chamber of the STM/S, XPS, or ARPES setup. They were cleaned from native oxide by annealing them to a sample temperature of 380 °C for 30 min and simultaneously exposing them to atomic hydrogen, generated by a thermal cracker (from MBE components) operated at 1700 °C with a hydrogen (H_2) pressure of 2×10^{-6} mbar. Bi was deposited for 10 min using an effusion cell (from MBE components). Metallic Bi grains were heated to 470 °C and the sample growth temperature was kept at $T_s = 250$ °C.

STM/S studies were performed at $T < 10$ K in a Sigma Infinity STM in constant current mode using electrochemically etched tungsten tips. STM images with negative (positive) sample bias represent filled-state (empty-state) imaging. For STS measurements, the differential conductance *dI/dV* was recorded simultaneously with tunneling current using a lock-in amplifier with an ac modulating nominal peak-to-peak signal $V_{ac} = 10$ mV and frequency = 1043 Hz.

XPS and ARPES measurements were performed at the FlexPES and BLOCH beamlines of the MAX IV Laboratory, Sweden. In *4d*, Sb *4d*, and Bi *5d* core levels were obtained at room temperature using a surface-sensitive photon energy of 130 eV with a pass energy of 5 eV. The spectra were background fitted using a Shirley background and deconvoluted using the Igor Pro software, assuming pseudo-Voigt functions; fitting parameters are included in the Supplemental Material (SM), Sec. VI [19]. For ARPES, the sample was cooled down to $T < 19$ K. The band dispersion was measured using linear polarized light, a Scienta DA30-L spectrometer, an x-ray spot size of 15×10 μm^2, and an energy resolution of <10 meV.

III. RESULTS AND DISCUSSION

Here, we start with a short investigation of the clean InSb(111)A surface and then focus on the surface properties characterized using STM, STS, XPS, and ARPES. Using combined surface science techniques and a holistic investigation, we have aimed to relate localized electronic structure to the large-scale electronic band dispersion.

A. Clean InSb(111)A surface—In-trimer (2 × 2) reconstruction

A large-scale STM image of the InSb(111)A surface after removal of the native oxide is shown in Fig. 1(a). The surface is mainly composed of large InSb terraces, the height of which is approx. 4.0 Å [Fig. 1(b)], similar to the InSb(111) interplanar distance found in literature (3.7 Å) [10]. The high-

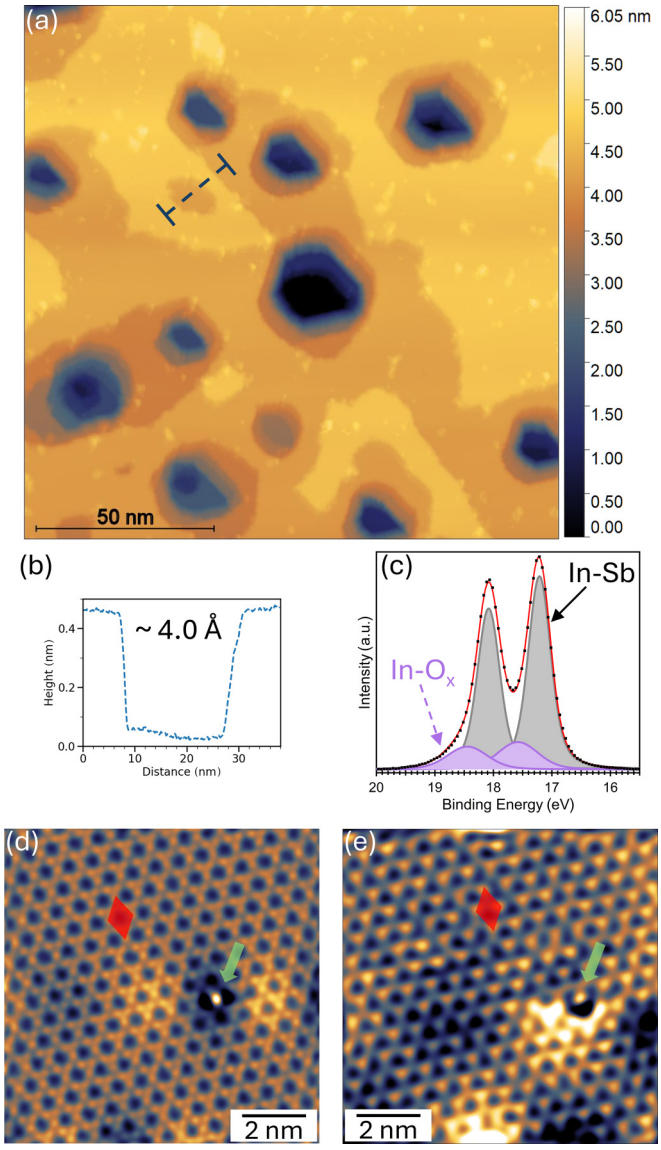


FIG. 1. (a) STM image of a clean InSb(111)A surface (V = +3.0 V, I = 100 pA), (b) height profile taken along the blue dashed line shown in (a), (c) In 4*d* core level spectra, two fitted components are indicated, and (d) high resolution empty (V = +1.0 V, I = 120 pA) and (e) filled state (V = −1.0 V, I = 110 pA) images; green arrows indicate the same surface defect in both the images and red rhombi highlight the surface reconstruction.

resolution empty and filled state STM images of the surface terrace are shown in Figs. 1(d) and 1(e), respectively. Additional bias-dependent STM images can be found in the SM Fig. S1. The empty state images mainly comprise In trimers with (2 × 2) reconstruction, highlighted with a red rhombus in Fig. 1(d). The (2 × 2) surface reconstruction of InSb(111)A has been previously understood by Bohr *et al.* as an In-vacancy buckling structure [24–26].

The chemical composition of the clean InSb surface was further investigated using synchrotron-based XPS. In *4d* core level spectra could be fitted using two doublet components, as shown in Fig. 1(c), where the main component at 17.2 eV binding energy (BE) is attributed to In-Sb

bonding. The smaller peak at 0.4 eV higher BE could be a convolution of a surface component and small amounts of In-oxide contributions like In(+1) and In(+3) [15]. The STM and XPS confirm a predominantly oxide-cleaned, (2 × 2) reconstructed InSb(111)A surface.

B. Bi/InSb(111)A surface

Bi was deposited at elevated sample temperature, as explained in the methods. The deposition at elevated temperatures facilitates Bi incorporation over thin film growth, as observed previously [15]. The STM image of the resulting surface, see Fig. 2(a), shows large-scale flat terraces with well-defined edges along ⟨110⟩ symmetry directions [highlighted with red dashed lines in Fig. 2(a)], with the angle between the edges being 120° and 60° (three- or sixfold rotational symmetry). The apparent height of the topmost surface termination is about 1.5 Å (as shown in the inset), while the step height of the terraces is still ∼4.0 Å. This means that the terrace structure is that of an InSb(111) facet, while Bi deposition is limited to the surface termination. The 1.5 Å height of the incorporated Bi is consistent with the reported thickness value of a one ML thin Bi(111) film along the [111] symmetry direction [14]. Mishima *et al.* computed the relaxed atomic structure for the InSb(111)A-(2 × 2) surface and reported the same atomic height of In and Sb atoms from the side view [25]. This could be the reason for the observed single atomic height of the layer of Bi atoms after incorporation into the InSb(111)A surface.

An atomically resolved STM image from a similar area is shown in Fig. 2(b), where two periodic features with different unit sizes and orientations can be seen. The larger part of the image has a homogeneous and densely packed (2 × 2) surface reconstruction along the ⟨110⟩ symmetry direction, which has also been reported before [27]. However, a $(2\sqrt{3} \times 2\sqrt{3})$-R30° surface reconstruction along the ⟨121⟩ direction is newly observed. It has limited coverage, as highlighted with a red dashed circle in Fig. 2(a), and can be seen in Fig. 2(b). Possibly because of an insufficient amount of Bi atoms being available during the limited deposition time for reaching complete ML coverage, the observed height of the (2 × 2) surface is about 1.5 Å above the bare InSb terrace and ∼53 pm above the $(2\sqrt{3} \times 2\sqrt{3})$-R30° surface, as shown in the line profile inset in Fig. 2(a). This apparent height difference between the two types of surface reconstruction could be due to structural differences between the two types of Bi superstructure or due to different electronic STM contrasts. Assuming that the observed (2 × 2) surface reconstruction contains one Bi atom per unit cell, as indicated by high-resolution STM images, we obtain a Bi coverage of 0.25 ML. However, the number can differ from the actual value due to the mixture of surface reconstructions and areas with only partial Bi coverage.

The large-scale STM images of the Bi/InSb(111)A surface confirm a long-range ordered sample surface. There is no indication of strain-induced dislocations from Bi deposition under the current sample treatment condition, as observed in Bi deposition on InSb(111)B and SiC substrates [8,13,14]. This highlights the suitability of InSb(111)A substrate for Bi incorporation and overgrowth. Furthermore, it is interesting

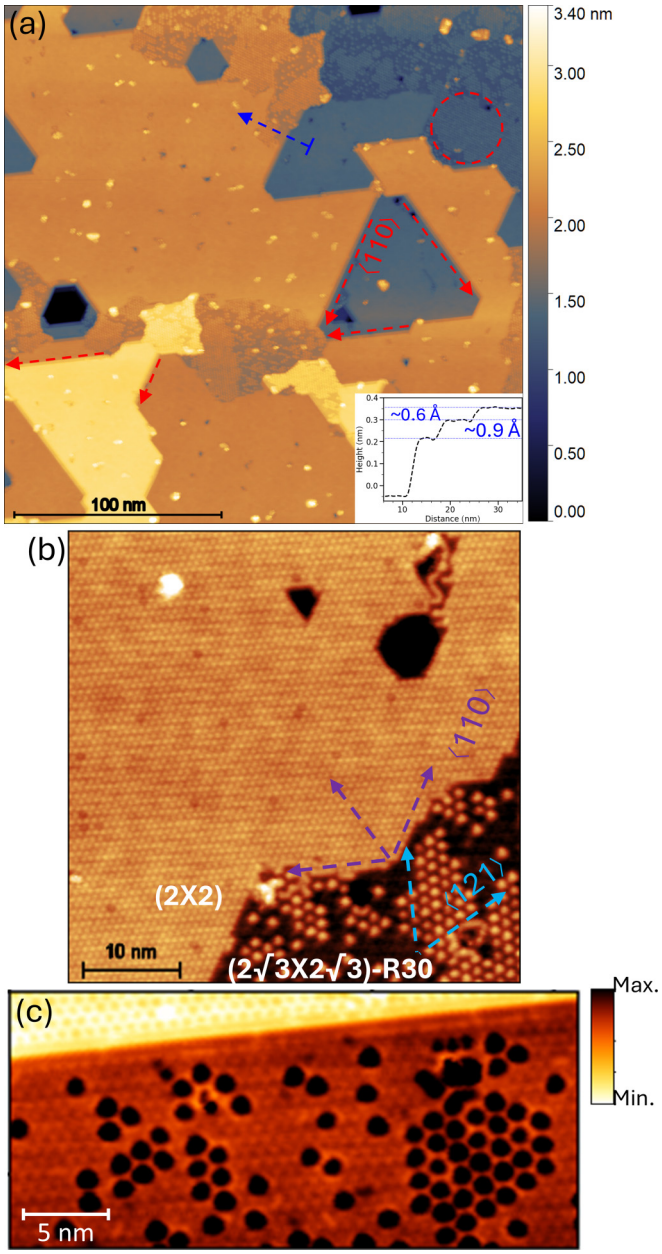


FIG. 2. (a) Empty state STM image of deposited Bi on InSb(111)A surface, height profile along the blue line is shown in the inset, (b) high-resolution image at the interface of different surface reconstructions of Bi/InSb(111)A, and (c) reverse contrast image to highlight the reconstruction of the InSb substrate underneath (red color), black circles being $(2\sqrt{3} \times 2\sqrt{3})$-R30°, with the above images taken at V = +3.0 V, I = 110 pA.

to note that the InSb(111) surface, which can be seen between isolated patches of the $(2\sqrt{3} \times 2\sqrt{3})$-R30° arrangement, still shows the In trimer (2 × 2) reconstruction of the InSb(111)A substrate, as observed in the reverse contrast STM image in Fig. 2(c).

C. Localized trimers in Bi/InSb(111)A-(2 × 2) surface

To better understand the electronic properties of the Bi surface reconstructions, the STM sample bias was varied from

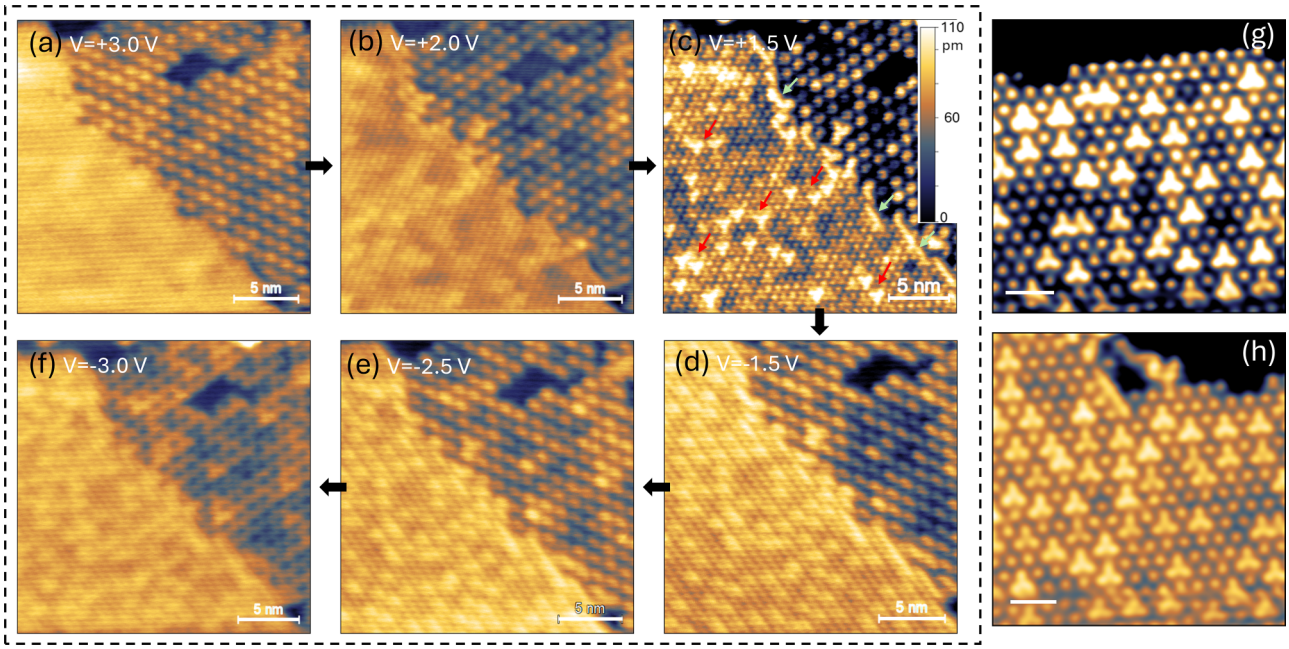


FIG. 3. (a)–(f) Enclosed in dashed line are the bias-dependent STM images of the Bi/InSb(111)A surface at the interface between two different surface reconstructions, varying from high positive voltage (empty states) to high negative voltage (filled states). Bi-trimer and edge states are indicated with red and green arrows, respectively, with the color scale in right top corner (scale bar is 5 nm in each image); (g),(h) inverse FFT filtered high-resolution STM images to highlight the Bi-trimer decorated reconstruction on the (2 × 2) surface; scale bar is 2 nm (all images taken at V = +1.5 V, I = 100 pA).

+3.0 V (empty state) to −3.0 V (filled state), as shown in Figs. 3(a)–3(f). An area with mixed surface reconstruction was decided. As the absolute bias decreases from higher to lower values, specific states become more pronounced, especially in the region of the (2 × 2) surface reconstruction and at the interface between both reconstructions, as highlighted by red and light green arrows, respectively, in Fig. 3(c). Particularly for small positive potential (+1.5 V), the pronounced states in the (2 × 2) region are in a triangular arrangement, as shown in Fig. 3(c). This triangular arrangement extends over three lattice points of the (2 × 2) reconstruction; thus we term these structures as trimers from now onward. Along with trimers, we also see a more enhanced contrast at the interface between (2 × 2) and ($2\sqrt{3} \times 2\sqrt{3}$)-R30° reconstructed areas in images with lower absolute sample bias, such as Figs. 3(c) and 3(d). The trimer and interface states fade away as we reach higher absolute bias values. Although the trimers can still be recognized in the images with higher negative bias [Figs. 3(d) and 3(e)], both the contrast and spatial resolution decrease. An STM image taken at ±1.5 V shows the local density of state (LDOS) of the surface integrated from the Fermi level (E_F) up to the energy of ±1.5 eV; thus the observed trimers and interface states must have a locally enhanced LDOS within this energy range.

It is known from STM literature that atomic defects or dopants and even adatoms can appear bright at one bias polarity and be hardly visible or even appear dark at the other one [28–30]. However, here the trimer and interface states are visible with bright contrast at certain sample voltages of both polarities and have fading contrast for higher voltages, also at both polarities, which strongly indicates that they have an electronic origin and are not due to surface topography. Furthermore, the largest apparent height of the trimer features, obtained in STM images taken at bias voltages resulting in the strongest contrast, is only 60 pm higher [in Fig. 3(c)] than that of the surrounding individual Bi features, which is much less than the apparent height of Bi adatoms measured by STM [11].

The trimer states are more clearly visible in the high-resolution STM images of Figs. 3(g) and 3(h), showing two different areas within the (2 × 2) reconstructed region, which have undergone postimage processing (fast Fourier transform). As mentioned above, each trimer extends over three lattice points of the periodic Bi-induced surface, i.e., the trimer points follow the symmetrical direction of the 2 × 2 surface reconstruction. At positions without trimers, the reconstructed surface shows one bright spot per (2 × 2) unit cell, interpreted as individual Bi atoms. In a trimer, three of these bright spots form a paired system where the STM image contrasts. Thus the surface LDOS is arranged in triangular geometry. The trimers are along the same orientation, meaning they have a threefold symmetry, in contrast to the sixfold symmetry of the hexagonal pattern of the (2 × 2) reconstruction. We relate this to the threefold symmetry of the adsorption site in the InSb zinc-blende (111) surface. The local arrangement of the trimers on the (2 × 2) reconstructed surface lacks long-range periodicity, but pairs of neighboring two or three trimers are slightly preferred, as confirmed by autocorrelation analysis (see SM Sec. 3 and Fig. S3 for more details). In a few cases, even overlapping trimers can be found. The local arrangement of the trimers is stable over time, i.e., the trimers are observed at the same positions in subsequent STM images (see Fig. 3), which excludes random fluctuations.

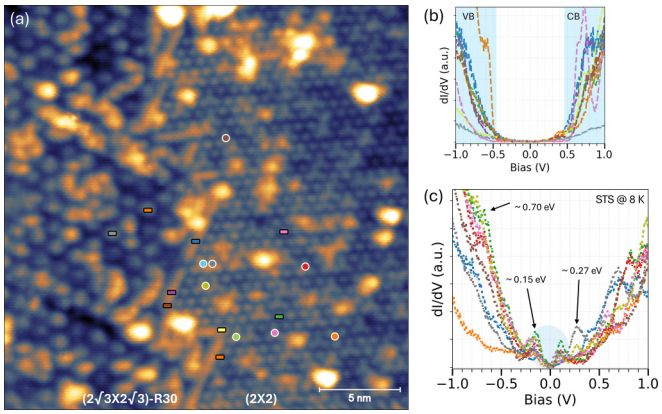


FIG. 4. (a) STM image with two Bi-induced surface reconstructions on InSb(111)A, (2×2) (right) and $(2\sqrt{3} \times 2\sqrt{3})$-R30 (left), and the interface between. Colored rectangles and circles mark the positions where STS data were taken in (b) and (c). (b) *dI/dV-V* spectra are taken at various positions on the surface, excluding trimers. Estimated valence band (VB) and conduction band (CB) positions are indicated. (c) *dI/dV-V* spectra obtained on Bi-induced trimers showing DOS peaks within the band gap (highlighted with a light blue circle).

Here, the trimers can be interpreted as localized states from three adjacent Bi atoms, resulting in perturbation of the otherwise constant surface potential of the Bi/InSb(111)A. Although this potential perturbation is periodic in limited areas, it lacks large-scale periodicity, which could be due to surface defects or incomplete Bi deposition. Even though the trimers are localized, nonperiodic features of enhanced DOS at the atomic scale do not show quantized behavior but instead give rise to additional bands, as STS and ARPES results discussed in later sections will confirm. Thus these trimers can be understood as correlated rather than discrete systems. Interestingly, the localized trimer states are only present in the (2×2) reconstructed surface areas and are absent from the less densely packed $(2\sqrt{3} \times 2\sqrt{3})$-R30° surface reconstruction.

D. Metallic DOS due to Bi trimers

We have employed scanning tunneling spectroscopy (STS) locally at different surface structures to probe their electronic DOS. The LDOS at specific energy is investigated by exploring differential conductivity *dI/dV* vs *V* [31,32]. For STS, we have chosen surface areas with various Bi arrangements, including the (2×2) reconstruction with and without trimers, the $(2\sqrt{3} \times 2\sqrt{3})$-R30° reconstruction, and the interface between these reconstructions, as shown in Fig. 4(a) and SM-S4. The *dI/dV-V* spectra from different surface structures are grouped in Figs. 4(b) and 4(c) according to the corresponding location in the surface as marked in Fig. 4(a). Most areas of the surface obtained after Bi deposition show an energy region with very low LDOS, extending from about −0.4 to +0.4 eV [highlighted in Fig. 4(b) and SM Fig. S5]. This energy interval is significantly larger than the expected band gap of InSb (∼ 0.23 eV at 7.5 K) [33], even if one considers a slight apparent broadening due to tip-induced band bending [34–36], and it remains unclear if this is due to Bi-induced band engineering or if the actual conduction and valence band onsets are not visible due to a very low LDOS close to the band edges. Interestingly, the observed energy window is consistent with the reported Bi-induced topological band gap (0.8 eV) from deposited hexagonal Bi on Si(111) and SiC substrates [8,10].

In contrast to the behavior of all other surface areas, the *dI/dV-V* spectra obtained at the positions of the trimers show distinct additional states within the apparent band gap at both sides of the Fermi level (which is at 0 V), as highlighted in Fig. 4(c). For negative sample bias, a prominent peak is found at about −150 meV. For positive sample bias, there are two prominent peaks at about 100 meV and 270 meV. Additional peaks at energies below 1.0 eV can be found in the valence band (at −0.7 eV) and the conduction band (at 0.7 and 0.8 eV) regions. The higher DOS of the trimers observed by STS for energies below 1 eV explains their enhanced contrast in STM images with small positive and negative sample bias: for larger absolute sample bias, the bulk conduction and valence bands with their high LDOS dominate the STM images, while the relevance of additional LDOS at energies below ±1 eV increases with decreasing sample bias, keeping in mind that STM images show the LDOS integrated from the Fermi level to the sample bias. The *dI/dV-V* spectra of the Bi-induced trimers show a finite LDOS within the entire band gap region, indicating metallic behavior. The almost linear V-shaped LDOS around 0 V also indicates metallic states in Bi nanostructures [1,16,37,38]. We will return to the Bi-induced trimers and their LDOS observed in STS in a later section when we discuss ARPES band dispersion.

E. Bi-Sb bonds

The chemical interaction between Bi and InSb(111)A surface was studied using XPS under similar sample treatment conditions. Overview spectra, including Sb *4d,* Bi *5d*, and In *4d* core levels, indicate successful Bi incorporation, compared to spectra from clean InSb, as shown in SM Fig. S6. The first step of Bi deposition was done at elevated sample temperature ($T_s = 250\,^{\circ}$C), followed by additional cycles under similar conditions. A subsequent Bi deposition step with the sample at room temperature and final annealing at $T_s = 250\,^{\circ}$C without Bi deposition was followed. The intensity of the Bi *5d* peak increases with every Bi deposition cycle, but, for the annealing step, it decreases due to Bi desorption from the surface (Fig. S6 of the SM). The asymmetry of the Bi *5d* peak suggests that a higher BE component dominates at the first deposition cycle, whereas a component at a lower BE increases upon the following cycles. Figure 5 compares deconvoluted Bi *5d* core level spectra, fitted with two doublet components corresponding to Bi-Sb (yellow colored) and Bi-Bi bonds (magenta colored), ΔBE ≈ 0.55 eV, consistent with our previous study on Bi/InSb(111)B [15] and with reported literature [11,39]. The XPS fitting parameters are presented in SM Table S1. The Bi-Sb bonds dominate in the initial Bi deposition cycle, whereas Bi-Bi bonds increase thereafter, explaining the layered growth of Bi. This is in contrast to Bi deposition on InSb(111)B, where the amount of Bi on the sample is self-limiting at elevated sample temperature [15]. The increase in Bi film thickness observed here could be because of a stronger interaction of evaporated Bi with Bi/InSb(111)A than with Bi/InSb(111)B. Thus, upon further

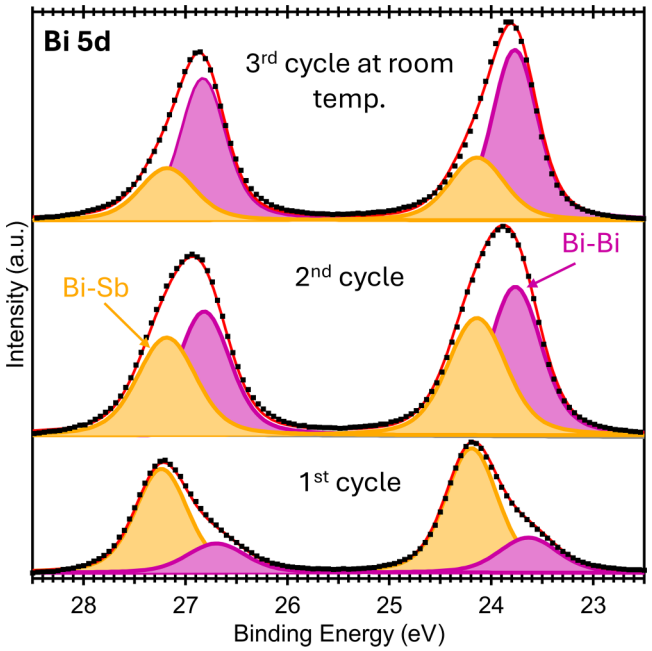


FIG. 5. Fitted Bi 5*d* core level spectra under various Bi deposition conditions; first and second cycles of Bi deposition were performed at elevated sample temperature 250 °C, followed by the third deposition cycle at room temperature (the spectral intensity is normalized for plotting).

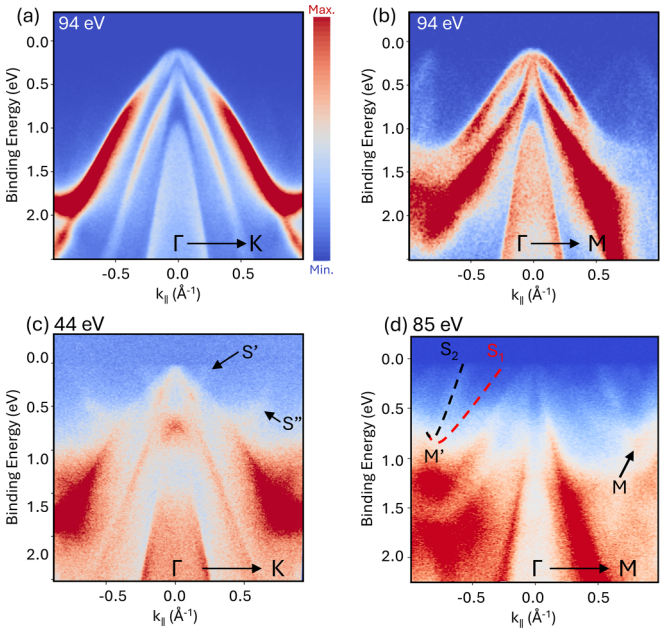


FIG. 6. ARPES band dispersion of cleaned InSb(111)A along (a) Γ-K and (b) Γ-M symmetry directions. (c), (d) Band dispersion with 0.35 ML Bi coverage, indicating SSs marked as S′ and S″ along Γ-K and S1 and S2 along Γ-M symmetry directions. Used photon energies are indicated.

Bi deposition on InSb(111)A (at $T_s = 250\,^{\circ}\mathrm{C}$), metallic Bi does not desorb simultaneously, resulting in an increasing Bi film thickness with subsequent deposition cycles. Here, the importance of the different polarities of the underneath substrate (Sb-terminated or In-terminated) in Bi incorporation is highlighted. Nevertheless, Bi-Sb remains stable under varying subsequent deposition conditions, as observed in both cases.

Importantly, we see no indication of bismuth bonding to indium in our XPS data. For the In *4d* core level, In-Bi bonding would be expected to result in a low BE shoulder [36]. In *4d* spectra obtained before and after Bi deposition are compared in SM Fig. S6(b), showing almost perfect overlap and the absence of a Bi-induced shoulder. Bi-In bonding is difficult to identify at the Bi *5d* core level, as it overlaps with the component due to Bi-Bi bonding [39]. Based on STM images and XPS analysis, the following Bi-incorporation mechanism can be proposed: upon initial deposition of Bi onto the clean InSb(111)A surface, Bi atoms adsorb at the In vacancy sites of the 2×2 reconstruction and bond to three neighboring Sb atoms underneath, which previously were missing a bonding partner. The incorporation of Bi on the vacancy sites naturally supports a Bi-induced (2×2) surface reconstruction, which is observed in the STM image. A schematic representation of the Bi incorporation and induced (2×2) surface reconstruction is included in SM Fig. S2.

F. Trimer-induced surface states

The ARPES band structure of clean InSb(111)A, centered around Γ and along Γ-K and Γ-M symmetry directions, is shown in Figs. 6(a) and 6(b). The valence band below the Fermi level (E_F, at 0 eV) has parabolic band dispersion and faint band folding from the (2×2) surface reconstruction, as shown in Fig. 6(b). After Bi deposition, new states are observed around the Γ point, crossing the E_F [Figs. 6(c) and 6(d)]. The states are marked as S′ and S″ along the Γ-K direction and S1 and S2 along the Γ-M symmetry direction and in the latter case also highlighted with dashed lines. A photon energy-dependent intensity plot taken at the M point is shown in SM Figs. S7b and S7c, where the dispersion intensity at 0.5 eV BE remains continual between 40 and 80 eV photon energy. Thus we can assign the new states along the Γ-M direction as surface states (SSs). As the SSs cross E_F, this indicates the emergence of Bi-induced metallic states on an Bi/InSb(111)A surface, in contrast to the band gap observed in pristine InSb(111)A [38]. Several reports on multilayer Bi(111) film and Bi crystal have observed similar SSs and have assigned them to metallic states with spin-polarized splitting or Rashba effect along the Γ-M symmetry direction [7,13,38,40,41]. Among those, the lowest Bi coverage (a one-bilayer thin Bi film) on the InSb(111)B surface was reported by Inbar *et al.,* presenting experimental ARPES and calculated density functional theory results, who identified similar SSs with the band splitting at Γ, attributed to strong Bi-substrate interaction [13]. Similarly, in our case, we assign the Bi-induced SSs from 0.35 ML coverage to Rashba splitting crossing E_F; the schematic is shown in SM Fig. S8. We calculate the Bi coverage of our sample from the measured intensities of the Bi *5d* and Sb *4d* core level spectra, according to an overlayer model as described in detail in SM Sec. 6 [13,14], amounting to ca. 0.35 ML (0.6 Å). Due to this low Bi coverage, the intensity of the Bi-induced band dispersion in Figs. 6(c) and 6(d) is low.

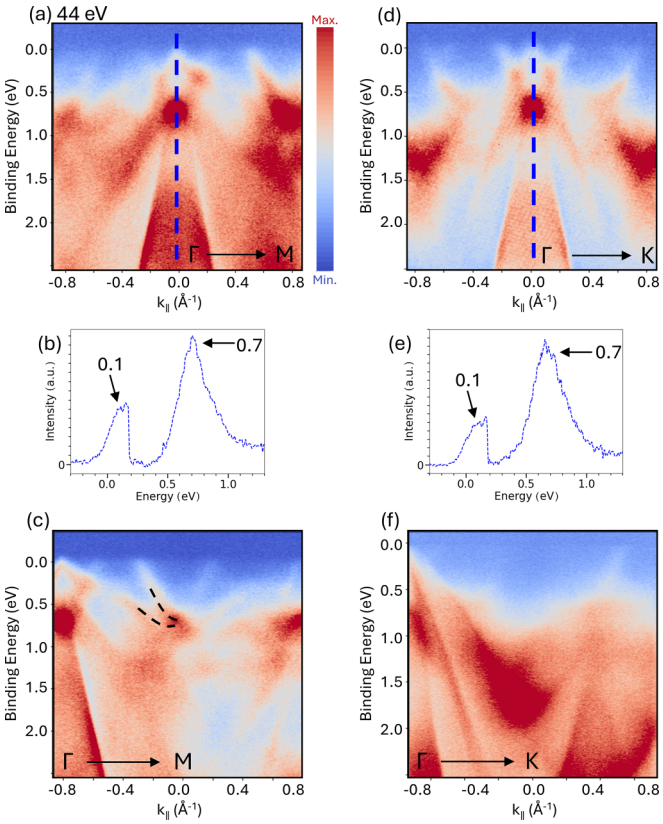


FIG. 7. ARPES band dispersion (hv = 44 eV) of Bi/InSb(111)A for 1.0 ML Bi coverage (a) along the Γ-M direction, (b) corresponding EDC along the Γ point, and (c) tilted sample to center around the M point; degenerate SSs are highlighted with black dashed lines. (d) Band dispersion along Γ-K, (e) corresponding EDC, and (f) band dispersion centered around the K point.

It has been observed previously that the deposition of a few additional ML of Bi would not affect the signature of Rashba splitting due to the strong Bi-substrate interaction and only impact the energy splitting between quantum well states, which can be observed after the deposition of more than 1 BL of Bi [13]. Thus we also deposited more Bi under similar sample treatment conditions to improve signal intensity, resulting in a Bi coverage of ca. 1 ML. Figure 7 shows the corresponding band dispersion along Γ-M and Γ-K direction. The surface state bands along Γ-M, the band splitting at the Γ point, and the band crossing at E_F can be seen more clearly now in Figs. 7(a) and 7(c). This further supports the above conclusion that the deposition of less than 1 ML of Bi on InSb(111)A results in spin-polarized splitting, according to the Rashba effect, at the Γ point [41,42]. A possible indication of Rashba splitting in the measured band dispersion is sketched in SM Fig. S8. The sample was then tilted along the Γ-M direction to investigate the M high symmetry point, as shown in Fig. 7(c). At the M point, we observe the SSs degenerating at just below 0.5 eV BE. Previous *ab initio* calculations and experimental work have associated the Bi-induced SSs degenerating at the M point as trivial topological states, including for Bi/InSb(111)B and H-passivated Bi(111) film [13,43,44].

We now discuss the relation between the localized trimers seen in STM images and their corresponding DOS peak observed by STS with the metallic SSs and band splitting observed in ARPES measurements. It is important to remember that the STS data showed metallic states only directly at the localized Bi trimers, while the surrounding surface was characterized by a band gap of around 0.7 to 1.0 eV. Thus the SSs observed in ARPES do not correspond to the Bi-induced isotropic (2 × 2) or the $(2\sqrt{3} \times 2\sqrt{3})$-R30° surface reconstruction in general, but they are coupled to the finite LDOS in STS taken at the trimers. In other words, the surface state splitting in ARPES can be associated with the observed localized trimers in the STM image. Here, we emphasize the role of localized electrons (as those forming the trimer contrast) in induced spin-polarized electronic band splitting or Rashba splitting. For a simplified quantitative comparison of the *dI/dV-V* spectra from STS data with the ARPES band dispersion, we have to take into account that only filled states can be investigated by ARPES (corresponding to negative sample bias in STS) and that the tunnel current in STM/S is lacking momentum resolution. We, therefore, evaluate the energy dispersion curve (EDC) of the ARPES data at the Γ point, i.e., for the smallest k values and at a symmetry point with high intensity. The Fermi-Dirac distribution needs to be subtracted from the EDC, as shown in SM Fig. S9. The EDC at the Γ point of the ARPES data of Fig. 7(a) and 7(d) is plotted in Fig. 7(b) and 7(e), showing peaks at around 0.1 and 0.7 eV; we assign the corresponding peaks to the SSs with Rashba splitting and bulk band states, respectively, as seen in the ARPES spectra in Figs. 7(a) and 7(b). Corresponding peak positions are also observed in the filled state region of the *dI/dV-V* spectra taken on trimers, i.e., at ca. −150 mV and −0.7 V. This simple comparison further confirms that the SSs observed in ARPES correspond to the localized Bi trimers imaged by STM.

Bi-induced localized trimer states have not been observed before in semiconductor surfaces. Periodic arrangements of Bi atoms in trimer geometry have been experimentally observed by STM for the Bi/Si(111) system and a peculiar type of Rashba splitting has been discussed for the Bi/Si(111)-$(\sqrt{3} \times \sqrt{3})$ surface with periodic Bi trimers, based on density function theory and ARPES results [6,45]. However, in that system, splitting was found for bands entirely below E_F in energy, while Rashba splitting of bands crossing the Fermi level is required for spintronic applications [46]. Also, efficient spintronic applications require high speed and low power consumption. InSb is a narrow band gap semiconductor with high electron mobility [15]. The combination of InSb with an ultrathin layer of Bi (0.35 ML here) shows strong indications of spin-polarized Rashba-Bychkov splitting at the Γ point with split bands crossing E_F, making this material system highly promising for future miniature and efficient spintronic application.

IV. CONCLUSION

In conclusion, we have demonstrated the incorporation of Bi in the InSb(111)A surface at elevated sample temperature. The surface is primarily flat and periodic with a mixed surface reconstruction, mainly (2 × 2) and in smaller areas

$(2\sqrt{3} \times 2\sqrt{3})$-R30°. STM images show Bi trimers in localized arrangements within the (2×2) reconstructed surface and interface states of enhanced LDOS at the border between different reconstructions. The localized trimers induce metallic SSs crossing the Fermi level at the Γ point, as confirmed by ARPES and *dI/dV-V* results. Furthermore, the metallic SSs show strong indications of the spin-polarized Rashba effect due to broken spatial inversion symmetry from strong Bi-substrate interaction. Thus we conclude that the localized trimers induce changes in the electronic band structure and Rasha splitting. Bi/InSb(111)A systems with localized electronic states presenting opportunities to explore band gap engineering, spin dynamics, and topological phenomena distinct from those in conventional quantum systems.

ACKNOWLEDGMENTS

The work was performed within the NanoLund center for nanoscience at Lund University and it was further supported by the Swedish Research Council (Vetenkapsrådet, Grant No. 2021–05627), the Knut and Alice Wallenberg Foundation (KAW, Grant No. 2017.0061), and the European Union through Horizon 2020 MSCA (Grant No. 945378, GenerationNano). We acknowledge the MAX IV Laboratory for beamtime on the FlexPES and BLOCH beamlines under Proposals No. 20220288 and No. 20231427, respectively. Research conducted at MAX IV, a Swedish national user facility, is supported by Vetenskapsrådet under Contract No. 2018–07152, the Swedish Governmental Agency for Innovation Systems (Vinnova) under Contract No. 2018–04969, and Formas under Contract No. 2019–02496. The authors want to acknowledge the support of the FlexPES and BLOCH beamline staff.

R.Y. conceptualizing, investigation, formal analysis, writing—original draft, and visualization; S.B. investigation, writing—review and editing; R.T. supervision, investigation, writing—review and editing.

DATA AVAILABILITY

The data that support the findings of this article are not publicly available. The data are available from the authors upon reasonable request.

[1] Y. Liu and R. E. Allen, Electronic structure of the semimetals Bi and Sb, Phys. Rev. B **52**, 1566 (1995).

[2] A. Takayama, T. Sato, S. Souma, T. Oguchi, and T. Takahashi, One-dimensional edge states with giant spin splitting in a bismuth thin film, Phys. Rev. Lett. **114**, 066402 (2015).

[3] I. K. Drozdov, A. Alexandradinata, S. Jeon, S. Nadj-Perge, H. Ji, R. J. Cava, B. A. Bernevig, and A. Yazdani, One-dimensional topological edge states of bismuth bilayers, Nat. Phys. **10**, 664 (2014).

[4] Z. Liu, C. X. Liu, Y. S. Wu, W. H. Duan, F. Liu, and J. Wu, Stable nontrivial Z2 topology in ultrathin Bi (111) Films: A first-principles study, Phys. Rev. Lett. **107**, 136805 (2011).

[5] Y. Ohtsubo, L. Perfetti, M. O. Goerbig, P. Le Fèvre, F. Bertran, and A. Taleb-Ibrahimi, Non-trivial surface-band dispersion on Bi(111), New J. Phys. **15**, 033041 (2013).

[6] M. H. Berntsen, O. Götberg, and O. Tjernberg, Reinvestigation of the giant Rashba-split states on Bi-covered Si(111), Phys. Rev. B **97**, 125148 (2018).

[7] T. Hirahara, T. Nagao, I. Matsuda, G. Bihlmayer, E. V. Chulkov, Y. M. Koroteev, P. M. Echenique, M. Saito, and S. Hasegawa, Role of spin-orbit coupling and hybridization effects in the electronic structure of ultrathin Bi films, Phys. Rev. Lett. **97**, 146803 (2006).

[8] F. Reis, G. Li, L. Dudy, M. Bauernfeind, S. Glass, W. Hanke, R. Thomale, J. Schäfer, and R. Claessen, Bismuthene on a SiC substrate: A candidate for a high-temperature quantum spin Hall material, Science **357**, 287 (2017).

[9] S. Sun, J.-Y. You, S. Duan, J. Gou, Y. Z. Luo, W. Lin, X. Lian, T. Jin, J. Liu, Y. Huang, Y. Wang, A. T. S. Wee, Y. P. Feng, L. Shen, J. L. Zhang, J. Chen, and W. Chen, Epitaxial growth of ultraflat bismuthene with large topological band inversion enabled by substrate-orbital-filtering effect, ACS Nano **16**, 1436 (2022).

[10] M. Zhou, W. Ming, Z. Liu, Z. Wang, P. Li, and F. Liu, Epitaxial growth of large-gap quantum spin Hall insulator on semiconductor surface, Proc. Natl. Acad. Sci. USA **111**, 14378 (2014).

[11] Y. Liu, S. Benter, C. S. Ong, R. P. Maciel, L. Björk, A. Irish, O. Eriksson, A. Mikkelsen, and R. Timm, A 2D bismuth-induced honeycomb surface structure on GaAs(111), ACS Nano **17**, 5058 (2022).

[12] M. Gmitra and J. Fabian, First-principles studies of orbital and spin-orbit properties of GaAs, GaSb, InAs, and InSb zinc-blende and wurtzite semiconductors, Phys. Rev. B **94**, 165202 (2016).

[13] H. S. Inbar, M. Zubair, J. T. Dong, A. N. Engel, C. P. Dempsey, Y. H. Chang, S. Nishihaya, S. Khalid, A. V. Fedorov, A. Janotti, and C. J. Palmstrøm, Structural inversion asymmetry in epitaxial ultrathin films of Bi(111)/InSb(111)B, Phys. Rev. Mater. **9**, 054202 (2025).

[14] C. Liu, Y. Zhou, G. Wang, Y. Yin, C. Li, H. Huang, D. Guan, Y. Li, S. Wang, H. Zheng, C. Liu, Y. Han, J. W. Evans, F. Liu, and J. Jia, Sierpiński structure and electronic topology in Bi thin films on InSb(111)B surfaces, Phys. Rev. Lett. **126**, 176102 (2021).

[15] R. Yadav, R. D. P. Maciel, S. Benter, C. S. Ong, O. Eriksson, A. Mikkelsen, and R. Timm, Bi trimers and self-limiting Bi-Sb interface formation upon Bi deposition on InSb(111)B surfaces, available SSRN (2024), doi:10.2139/ssrn.5059709.

[16] R. Canyellas, C. Liu, R. Arouca, L. Eek, G. Wang, Y. Yin, D. Guan, Y. Li, S. Wang, H. Zheng, C. Liu, J. Jia, and C. Morais Smith, Topological edge and corner states in bismuth fractal nanostructures, Nat. Phys. **20**, 1421 (2024).

[17] R. Stühler, F. Reis, T. Müller, T. Helbig, T. Schwemmer, R. Thomale, J. Schäfer, and R. Claessen, Tomonaga–Luttinger liquid in the edge channels of a quantum spin Hall insulator, Nat. Phys. **16**, 47 (2020).

[18] L. Aggarwal, P. Zhu, T. L. Hughes, and V. Madhavan, Evidence for higher order topology in Bi and $Bi_{0.92}Sb_{0.08}$, Nat. Commun. **12**, 4420 (2021).

[19] See Supplemental Material at http://link.aps.org/supplemental/10.1103/mp9b-hgz1 for biased dependent STM images of clean InSb(111)A, Bi-incorporation model, autocorrelation function, additional STS on trimers, core-level XPS spectra, XPS fitting parameters and thickness estimation, photon energy dependent surface states, schematics of Rashba splitting, and analysis of energy dispersion curve. The Supplemental Material also contains the following references: [14,15,20–23,42].

[20] M. Mohai and I. Bertti, Calculation of overlayer thickness on curved surfaces based on XPS intensities, Surf. Interface Anal. **36**, 805 (2004).

[21] J. E. Castle, in *Practical Surface Analysis by Auger and X-ray Photoelectron Spectroscopy*, edited by D. Briggs and M. P. Seah (John Wiley and Sons Ltd, Chichester, 1983), p. 533, Surf. Interface Anal. **6**, 302 (1984).

[22] H. Shinotsuka, S. Tanuma, C. J. Powell, and D. R. Penn, Calculations of electron inelastic mean free paths. XII. Data for42 inorganic compounds over the 50 eV to 200 keV range withthe full Penn algorithm, Surf Interface Anal. **51**, 427 (2018).

[23] S. M. Sze and K. K. Ng, Appendix F Properties of Important Semiconductors, in *Physics of Semiconductor Devices* (John Wiley & Sons, 2006), p. 789.

[24] J. Bohr, R. Feidenhans'l, M. Nielsen, M. Toney, R. L. Johnson, and I. K. Robinson, Model-independent structure determination of the InSb(111)2 × 2 surface with use of synchrotron x-ray diffraction, Phys. Rev. Lett. **54**, 1275 (1985).

[25] T. Mishima and T. Osaka, Profile imaging of the InSb{111}A,B-(2×2) surfaces, Surf. Sci. **395**, L256 (1998).

[26] M. Nishizawa, T. Eguchi, T. Misima, J. Nakamura, and T. Osaka, Structure of the InSb(111)A $-(2\sqrt{3}\times 2\sqrt{3})-R30^{\circ}$ surface and its dynamical formation processes, Phys. Rev. B **57**, 6317 (1998).

[27] S. Cho, Y.-H. Um, Y. Kim, George, K. L. Wong, J. B. Ketterson, J.-I. Hong, and G. K. L. Wong, Bi epitaxy on polar InSb(111)A/B faces, J. Vac. Sci. Technol. A **20**, 1191 (2002).

[28] P. Ebert, Nano-scale properties of defects in compound semiconductor surfaces, Surf. Sci. Rep. **33**, 121 (1999).

[29] P. M. Koenraad and M. E. Flatté, Single dopants in semiconductors, Nat. Mater. **10**, 91 (2011).

[30] N. Sato, T. Nagao, and S. Hasegawa, Two-dimensional adatom gas phase on the Si(111) $-\sqrt{3}\times\sqrt{3}-$ Ag surface directly observed by scanning tunneling microscopy, Phys. Rev. B **60**, 16083 (1999).

[31] R. M. Feenstra, Tunneling spectroscopy of the (110) surface of direct-gap III-V semiconductors, Phys. Rev. B **50**, 4561 (1994).

[32] Y.-P. Liu, L. Södergren, S. Fatemeh Mousavi, Y. Liu, F. Lindelöw, E. Lind, R. Timm, and A. Mikkelsen, Low temperature scanning tunneling microscopy and spectroscopy on laterally grown $In_xGa_{1-x}As$ nanowire devices, Appl. Phys. Lett. **117**, 163101 (2020).

[33] C. L. Littler and D. G. Seiler, Temperature dependence of the energy gap of InSb using nonlinear optical techniques, Appl. Phys. Lett. **46**, 986 (1985).

[34] R. Timm, R. M. Feenstra, H. Eisele, A. Lenz, L. Ivanova, E. Lenz, and M. Dähne, Contrast mechanisms in cross-sectional scanning tunneling microscopy of GaSb/GaAs type-II nanostructures, J. Appl. Phys. **105**, 53 (2009).

[35] M. Hjort, S. Lehmann, J. Knutsson, R. Timm, D. Jacobsson, E. Lundgren, K. A. Dick, and A. Mikkelsen, Direct imaging of atomic scale structure and electronic properties of GaAs wurtzite and zinc blende nanowire surfaces, Nano Lett. **13**, 4492 (2013).

[36] Z. Qu, Y. Sugawara, and Y. Li, Influence of tip-induced band bending on tunnelling spectra of semiconductor surfaces, Nanotechnology **18**, 44015 (2007).

[37] J. T. Dong, H. S. Inbar, C. P. Dempsey, A. N. Engel, and C. J. Palmstrøm, Strain solitons in an epitaxially strained van der waals-like material, Nano Lett. **24**, 4493 (2024).

[38] S. Yaginuma, K. Nagaoka, T. Nagao, G. Bihlmayer, Y. M. Koroteev, E. V. Chulkov, and T. Nakayama, Electronic structure of ultrathin bismuth films with A7 and black-phosphorus-like structures, J. Phys. Soc. Jpn. **77**, 014701 (2007).

[39] K. Szamota-Leandersson, M. Leandersson, M. Göthelid, and U. O. Karlsson, Correlated development of a (2 × 2) reconstruction and a charge accumulation layer on the InAs(111)-Bi surface, Surf. Sci. **605**, 12 (2011).

[40] H. Du, X. Sun, X. Liu, X. Wu, J. Wang, M. Tian, A. Zhao, Y. Luo, J. Yang, B. Wang, and J. G. Hou, Surface Landau levels and spin states in bismuth (111) ultrathin films, Nat. Commun. **7**, 10814 (2016).

[41] Y. M. Koroteev, G. Bihlmayer, J. E. Gayone, E. V. Chulkov, S. Blügel, P. M. Echenique, and P. Hofmann, Strong spin-orbit splitting on Bi surfaces, Phys. Rev. Lett. **93**, 046403 (2004).

[42] T. Hirahara, K. Miyamoto, I. Matsuda, T. Kadono, A. Kimura, T. Nagao, G. Bihlmayer, E. V. Chulkov, S. Qiao, K. Shimada, H. Namatame, M. Taniguchi, and S. Hasegawa, Direct observation of spin splitting in bismuth surface states, Phys. Rev. B **76**, 153305 (2007).

[43] I. N. Yakovkin, Dependence of the band structure of Bi(111) bilayers on lattice constant and spin-orbit splitting induced by a H monolayer, J. Phys. Chem. Solids **129**, 277 (2019).

[44] T.-R. Chang, Q. Lu, X. Wang, H. Lin, T. Miller, T.-C. Chiang, and G. Bian, Band topology of bismuth quantum films, Crystals **9**, 510 (2019).

[45] K. Sakamoto, H. Kakuta, K. Sugawara, K. Miyamoto, A. Kimura, T. Kuzumaki, N. Ueno, E. Annese, J. Fujii, A. Kodama, T. Shishidou, H. Namatame, M. Taniguchi, T. Sato, T. Takahashi, and T. Oguchi, Peculiar rashba splitting originating from the two-dimensional symmetry of the surface, Phys. Rev. Lett. **103**, 156801 (2009).

[46] N. V. Denisov, A. A. Alekseev, O. A. Utas, S. G. Azatyan, A. V. Zotov, and A. A. Saranin, Bismuth–indium two-dimensional compounds on Si(111) surface, Surf. Sci. **651**, 105 (2016).